Asia Pacific Science Press

Journal of Advances in Engineering and Technology
ISSN(O):3005-7507
ISSN(P):3005-7493
Vol. 2 No.2 (2025)

Synthesis of Cobalt Doping Titanium Dioxide Fiber Supported by Reduced Graphene Oxide for Photocatalytic Degradation of Toluene in Air

Guilan Gao[1], Xiran Zhang[1], Li Zhang[1], Shuai Chen[1]*, Pinnan Li[2]*

1.School of Minerals and Environmental Engineering, Shanghai Polytechnic University, Shanghai, 201209, China
2. UMR 8000 CNRS, Insitut de Chimie Physique, Université Paris-Saclay, Orsay, 91400, France

Corresponding author: Shuai Chen , chenshuai@sspu.edu.cn; Pinnan Li , pinnan.li@universite-paris-saclay.fr

Copyright: 2025 Author(s). This is an open-access article distributed under the terms of the Creative Commons Attribution License (CC BY-NC 4.0), permitting distribution and reproduction in any medium, provided the original author and source are credited, and explicitly prohibiting its use for commercial purposes.

Abstract: Titanium dioxide has been widely used for photocatalytic degradation of organic pollutants in air, while problems like low utilization rate of sunlight and easy recombination of photogenerated electrons and holes are the main drawbacks for its application. In this study, a combination of Co doping and graphene supporting was used to synthesize cobalt doping titanium dioxide fiber supported by reduced graphene oxide (Co-TiO_2/RGO) using processes including electrospinning, heating and freeze-drying. The structural and textural features of Co-TiO_2/RGO were characterized by different techniques, and toluene was used as a model pollutant to test its photocatalytic performance. Results show that Co-TiO_2 is uniformly dispersed in reduced graphene oxide and the specific surface area of Co-TiO_2/RGO is higher than that of TiO_2 and Co-TiO_2. Further, under the conditions of Co doping amount of 1%, calcination of 600℃ for 4 h, gas residence time of 100 min, relative humidity of 100%, and the Co-TiO_2 loading amount of 1 g, the degradation percentage of toluene by Co-TiO_2/RGO was the highest, up to 99.1%. This study confirms the possibility of synthesizing Co-TiO_2/RGO for the degradation of organic pollutants in air.

Keywords: Titanium Dioxide; Electrospinning; Photocatalytic Degradation; Toluene

Published: May 19, 2025

DOI: https://doi.org/10.62177/jaet.v2i2.349

1.Introduction

Volatile organic compounds (VOCs) in air have aroused wide concern because of their great variety and harm [1]. Among these, toluene is one of the most representative substances, which is toxic and carcinogenic, may cause serious damage to the nervous system and internal organs [2]. Photocatalytic oxidation, with the advantages of few by-products, and easy to operate, is currently one of the widely used methods to treat VOCs in air. The commonly used photocatalysts mainly include TiO_2 [3], g-C_3N_4 [4], BiOBr [5] etc., among which TiO_2 is one of the promising photocatalysts due to its strong photocatalytic ability and cost-effectiveness [6]. However, problems, such as large forbidden band gap, only being excited under UV-light, and low specific surface area, hinder its application [7].

As so far, many methods have been used in the modification of TiO_2. For example, H_2 could be employed to manufacture oxygen vacancy, which can decrease the band gap of TiO_2 [8]. What's more, doping metal or non-metal elements is also a promising idea, such as S doping [9], Cu doping [10], and even Co-doping [11]. Karafas et al. [12] prepared cobalt-doped TiO_2

array film, and found that the incorporation of Co improved the absorption of visible light and promoted the separation of photo-generated electro-hole pairs, leading to the better photocatalytic reduction performance compared with the film of TiO_2. About the problem of carrier recombination, Z-scheme heterojunction could be used to promote the separation of photoexcited carriers and reduce their recombination efficiency, leading to the enhancement of photocatalyst [13]. Additionally, coupling TiO_2 with semiconductors [14], and the recombination with carbon-based materials like carbon nanotubes [15], graphite oxide [16], and graphene [17] are also effective to enhance its activity. Because of the good conductivity due to the unique structure of graphene, it is of great interest to synthesize semiconductor-graphene [18]. Song et al. [19] used poly(3-hexylthiophene) (P3HT) to modify graphene, and added TiO_2 powder to the P3HT/graphene solution to form a P3HT/TiO_2/graphene composite. The presence of graphene improves the charge transport capacity, reduces the e^--h^+ recombination rate and further enhances its light catalytic activity of TiO_2. In addition, graphene combined with metal-modified TiO_2 has shown the stable and efficient photocatalytic degradation property. Xie et al. [20] prepared graphene oxide/TiO_2–Bi_2WO_6 to degrade ethylene, and found that the catalytic property of TiO_2–Bi_2WO_6 was significantly improved. However, the aggregation of TiO_2 or metal doped TiO_2 particles will lead to a decrease of the reactivity. Electrospinning has been a worth-trying way to synthesize TiO_2 [21-24], especially in the area of photocatalysis, due to its cost-effectiveness, and controlling of fiber dimensions which can get a larger surface area and then enhance the photocatalytic activity, and so on in a similar fashion.

So, in this work, the electrospinning was employed to compound TiO_2, which can successfully reduce the agglomeration of TiO_2 particles. Moreover, after Co-doping, the biggish band gap, one of the greatest Achille's heels of TiO_2, could be solved and more visible light can be absorbed. The graphene can promote the transfer of electrons under the effect of its high conductivity, so the recombination of carriers could be restrained [25-27]. In the end, toluene was chosen as a typical pollutant to test the catalytic activity of this photocatalyst.

2.Results and Discussion

2.1 Morphology, phase and optical characterization

Figure 1. XRD spectra of TiO_2/RGO and 1% Co-TiO_2/RGO

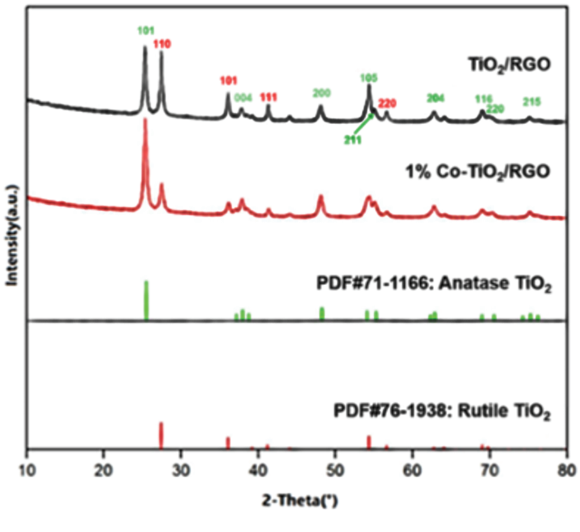

To explore the meaning of science behind the 1% Co-TiO_2/RGO which was synthesized by the electrospinning, a series of characteristics have been tested. First of all, the X-ray diffraction (XRD) patterns of the 1% Co-TiO_2/RGO have shown in Figure 1, suggesting that the prepared samples, TiO_2/RGO and 1% Co-TiO_2/RGO, both remain the structure of TiO_2. In other words, the 1% Co element could not change the formation of TiO_2. Compared with the work done by DeawAphairaj [28], a Rutile TiO_2 emerged after calcined at the temperature of 600°C. What's more, to examine the states of the product 1% Co-TiO_2/RGO, the X-ray photoelectron spectroscopy (XPS) was monitored in Figure 2. In Figure 2(a), the 284.60 eV is assigned to the C-C sp^2, and the 286.67 eV and 288.52 eV are represented the C-O-C and O-C=O, respectively. It means that the GO is not exactly reduced to graphene, and still have some functional groups which containing oxygen. In Figure 2(b), the peaks at 458.98 eV, 464.68 eV show a feature of TiO_2, but with a little red shift compared to the standard TiO_2 [29, 30]. It is a result of the Co doping, decreased the electron density on Ti^{4+}. After modified by Co element, the Ti^{3+} emerges at the peaks of 457.29 eV, 462.99 eV, which means oxygen vacancy was fabricated [31]. As shown in the Figure S2, the Co element can be observed at the peaks of 781 eV, 787 eV, 797 eV and 803 eV. The peaks reported at 781 eV and 797 eV corresponding to the Co^{2+} $2p^{3/2}$ and Co^{2+} $2p^{1/2}$, respectively. And the ones at 787 eV and 803 eV are satellite peaks which are on behalf of the formation of $CoTiO_3$ [32-34]. In conclusion, Co element successfully intercalated in the lattice of TiO_2.

Figure 2. XPS spectra of C 1s (a), Ti 2p (b) of 1% Co-TiO_2/RGO.

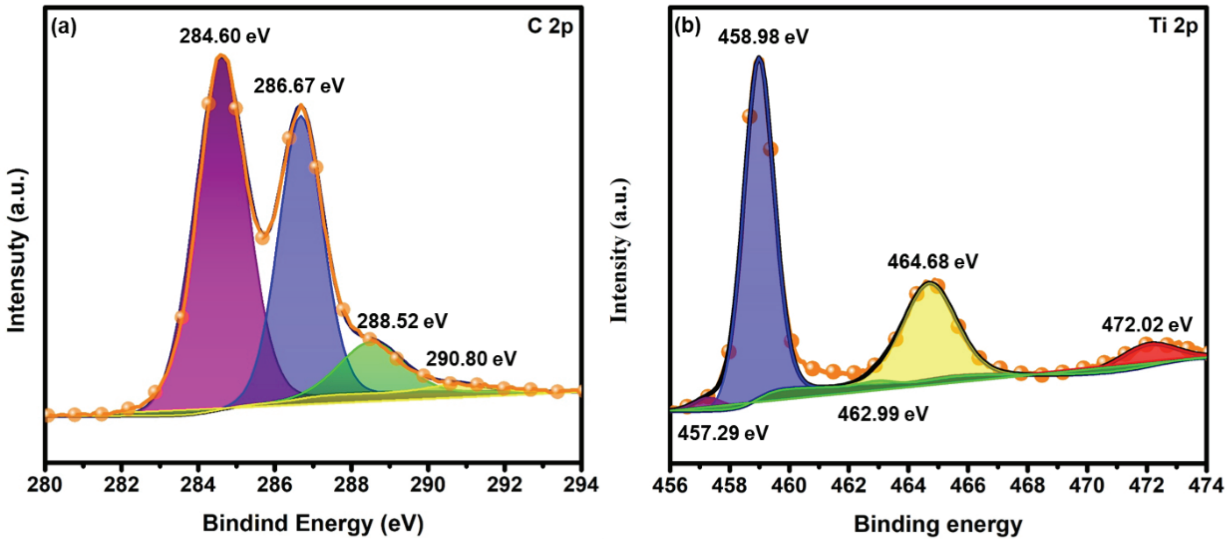

The SEM results of 1% Co-TiO_2/RGO is shown in Figure 3a-c. The morphology of Co-TiO_2 fiber is rod-like structure, with regular shapes and uniform protrusions on the surface. The RGO sheet is almost covered by the Co-TiO_2 rod-shaped particles trimly and uniformly as a result of the interaction between the RGO and TiO_2. What's more, the EDS figures, Figure 3d-f, show that the Co element anchoring in the TiO_2 fiber structure, so the result of EDS and XRD can corroborate each other.

Figure 3. SEM (a, b, c) and SEM-EDS (d, e, f) results of Co-TiO_2/RGO.

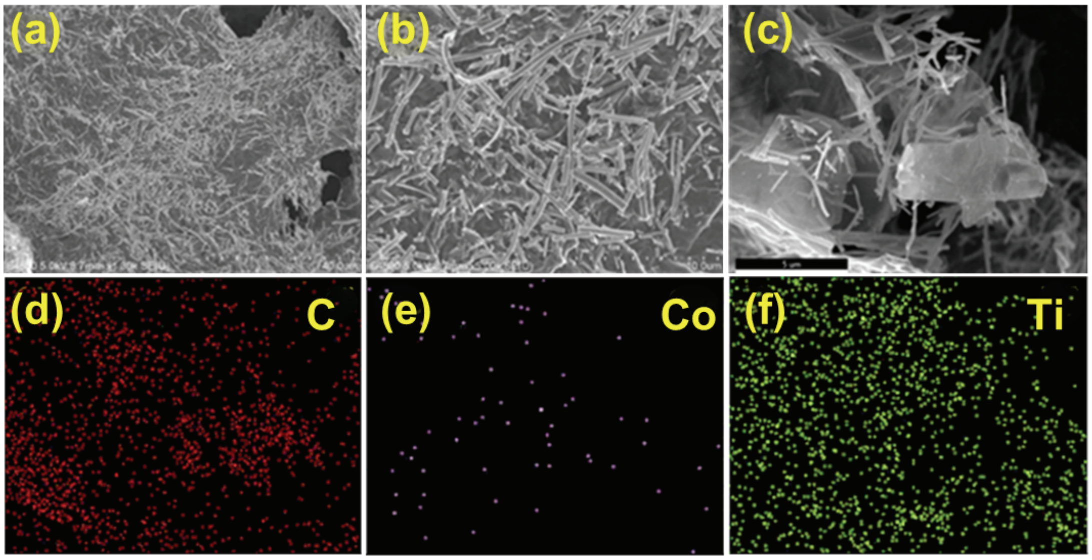

Figure 4 and Table S1 show the N_2 adsorption/desorption results and the pore size results of TiO_2 (a), Co-TiO_2 fibers (b) and Co-TiO_2/RGO (c). All the samples exhibit IV-type isotherms with H3-type hysteresis loops which demonstrates the present of mesoporous. As shown in Table S1, the specific surface area of the samples could obtain an obvious increasing after loading onto RGO, because the photocatalysts uniformly disperse onto the surface of RGO. It could let more reactive centers expose and improve its catalytic activity.

Figure 5 is the UV-vis absorption spectra of the samples at different calcination temperatures. It can be seen that the absorption edge of all samples has a significant red shift compared with TiO_2 calcined at the temperature of 500°C, showing that the addition of Co element can effectively extend the light absorption to the visible light range. This is because the changes of electronic transition. Due to the doping of Co, not only the Ti3d but also the Co3d can become conduction band when O2p become valence band. What's more, the electrons can also excite from Co3d-t_{2g} to Co3d-e_g. In summary, the long wavelength light can be absorbed [35-38]. Specifically, due to the influence of the wide band gap, TiO_2 has a significantly low light applicability, and as a result, the electrons can only be excited under the UV light. However, after the introduction of Co element, an impurity level emerged, which could expand the light absorption of TiO_2, because the edge of the band tail is extended into the forbidden band. The samples with Co doping which is calcined at the temperature of more than 500°C has an obvious blue shift compared with the one calcined at 500°C. This is the reason that the rutile phase of TiO_2 was created after calcined at the temperature of 600°C [39].

Figure 4. N_2 adsorption/desorption of TiO_2 (a), Co-TiO_2 (b), Co-TiO_2/RGO (c).

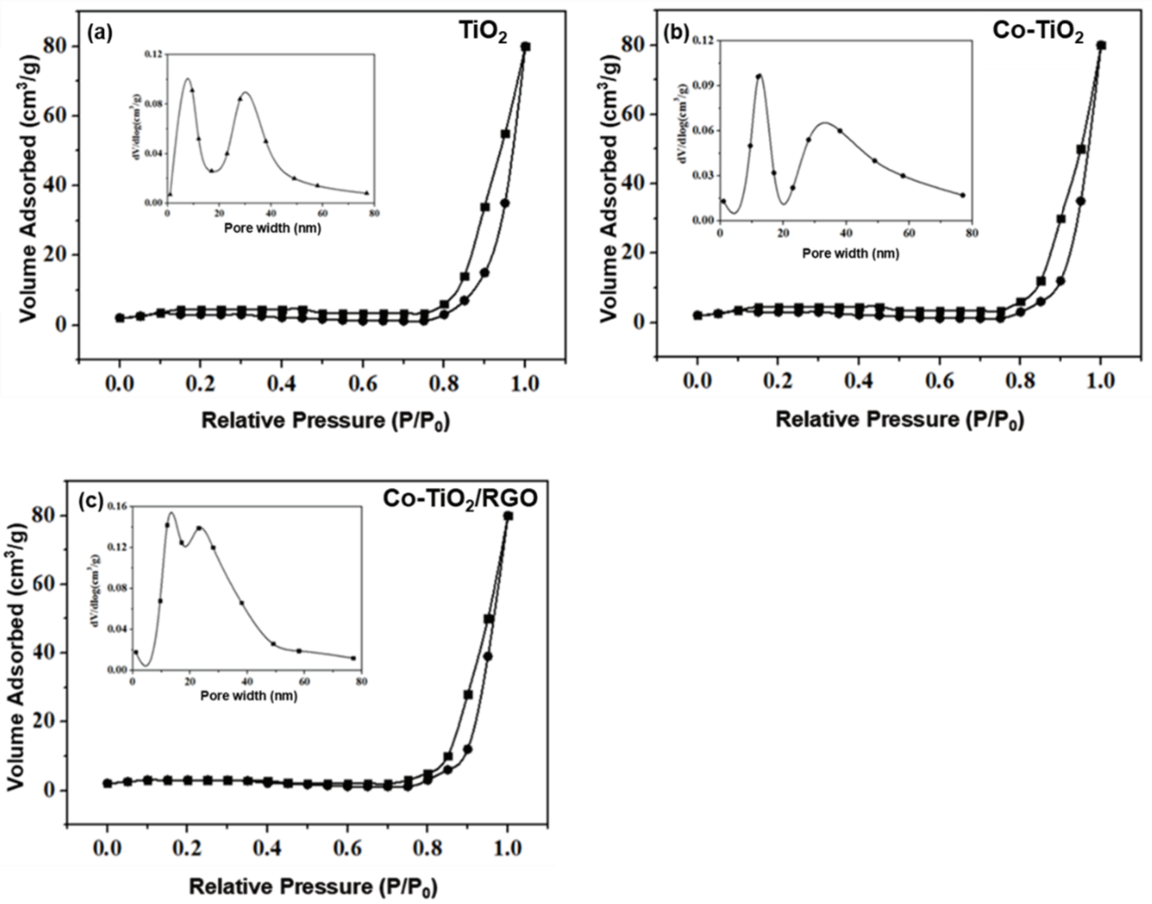

Figure 5. The UV-vis absorption spectra.

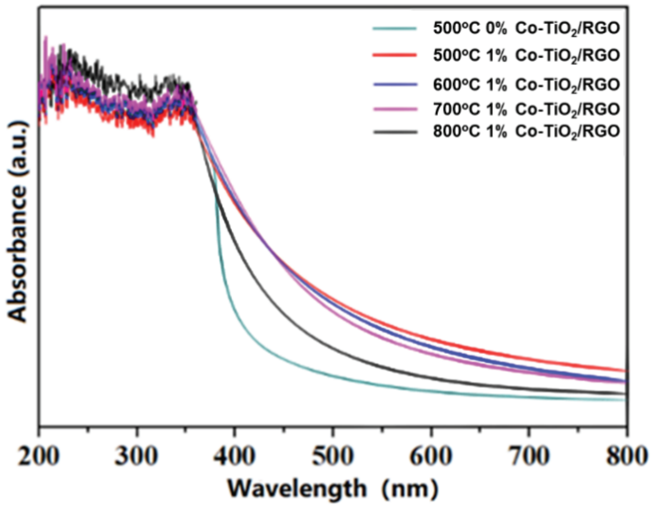

2.2 Photocatalytic degradation of toluene

Figure 6a shows the effects of Co-TiO_2/RGO photocatalysts with Co/TiO_2 molar ratios of 0, 0.005, 0.010, 0.015, and 0.020 on the degradation of toluene under the conditions of calcination at 500°C and degradation for 40 minutes. As the Co doping ratio increases, the photocatalytic performance of Co-TiO_2/RGO firstly increases and then decreases. When the molar ratio of Co: TiO_2 = 1: 100, the degradation performance of toluene was the best, reaching 82.6%. With a further increase of the Co doping ratio, the degradation efficiency does not increase but decrease. The photocatalytic activities of Co-TiO_2 in low concentration were higher than the non-doping TiO_2 samples. When the concentration of Co exceeds 2.5%, the photocatalytic rate was lower than non-doping TiO_2. This is because the excess dopants would lead to photon scattering [40].

Figure 6. Degradation of toluene with different Co doping (a), calcination temperatures (b), gas residence time (c), relative humidity (d), and catalysts.

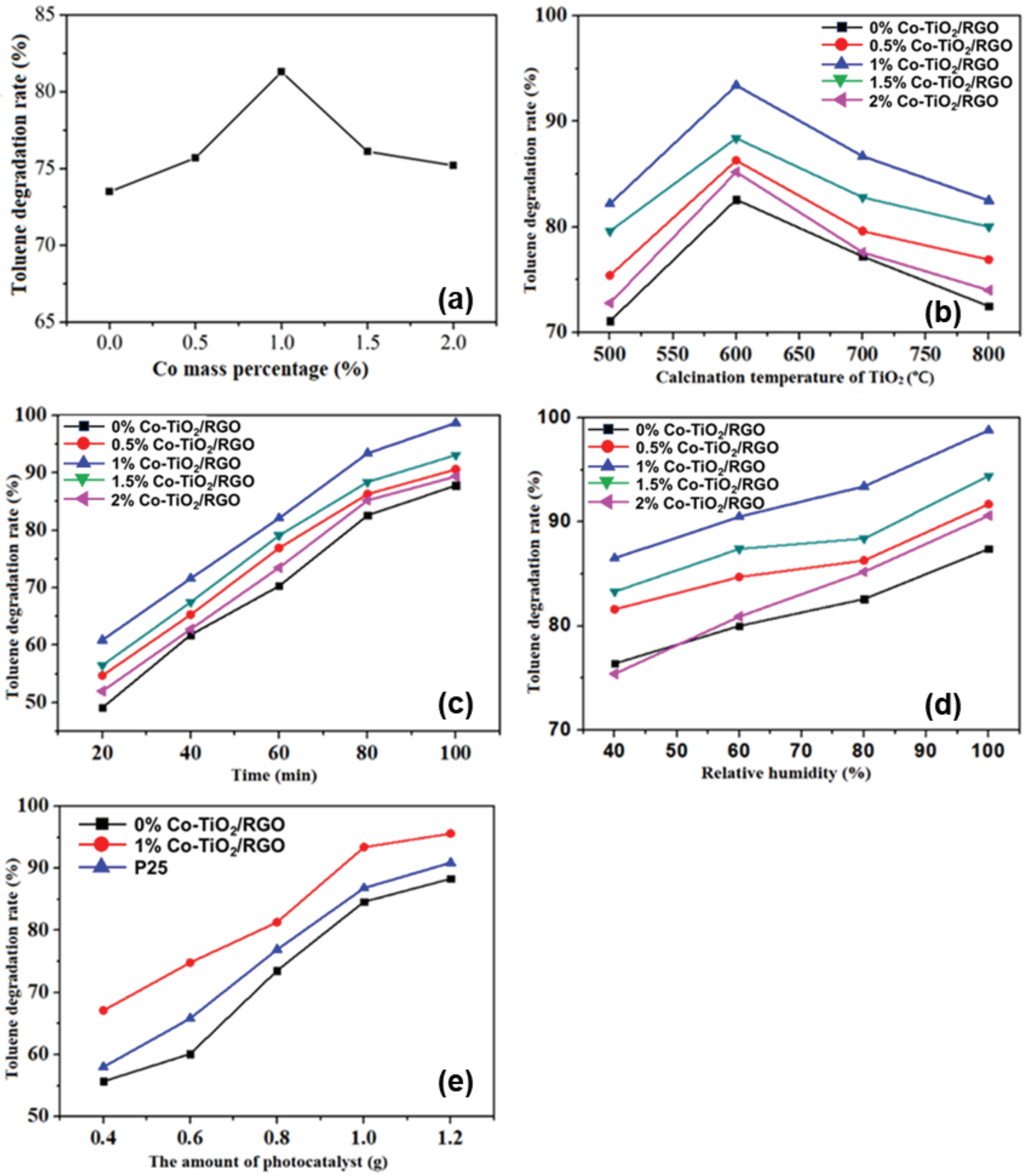

Figure 6b shows the degradation performances of toluene, in 60 min, by catalysts synthesized with different Co/TiO_2 molar ratios at different calcination temperatures. With the increase of calcination temperature, the photocatalytic performance of Co-TiO_2/RGO first increases and then decreases. The best degradation performance was reached when the calcination temperature is 600°C, and 1% Co-TiO_2/RGO, being 93.4%. When the calcination temperature is lower than 600°C, the PVP fiber is not completely carbonized, and the organic components attach to the Co-TiO_2 fiber, hindering the contact between the catalyst and light, thereby reducing the performance of photocatalytic degradation of toluene. When the calcination temperature is higher than 600°C, the rutile TiO_2 is formed and it can make the activity of the catalyst decline due to being unable to prevent the recombination of the carriers [41].

Figure 6c shows the degradation of toluene by photocatalysts synthesized with different Co/TiO_2 molar ratios at a calcination temperature of 600°C under different gas residence times. The photocatalytic performance of Co-TiO_2/RGO gradually increases with the increase of gas residence time. After 80 min, the degradation percentage of toluene infinitely approaches 100%, showing that with the increase of gas residence time, the photocatalytic reaction of Co-TiO_2/RGO with toluene will be completed. However, considering the cost, practicality and other factors, 100 minutes of degradation should be enough.

Figure 6d shows the effect of relative humidity on the degradation of toluene in 60 min, by Co-TiO_2/RGO synthesized under the conditions of calcination at 600°C. As the relative humidity increases, the catalytic activity of Co-TiO_2/RGO increases gradually, showing that the increasing of relative humidity is positively correlated with the degradation rate of toluene. The increase can enhance the activity of the catalyst hydroxyl radicals, thereby improving the photocatalytic activity of the catalysts. The degradation percentage of 1% Co-TiO_2/RGO for toluene increased from 86.5% to 99.1%.

Figure 6e shows the effect of TiO_2/RGO, 1% Co-TiO_2/RGO, and TiO_2 on the degradation of toluene under conditions of calcination at 600°C and degradation for 40 min. The 1% Co-TiO_2/RGO has the highest degradation percentage, reaching 95.6%, showing the loading improves the photocatalytic reaction of toluene. Nevertheless, considering the cost and practicability, the loading of the Co-TiO_2 should be selected at about 1 g.

Table 2 lists the removal values of toluene reported in literature using different materials. The data indicates that the Co-TiO_2/RGO system shows competitive removal performance of toluene in shorter reaction time.

2.3 The mechanism of photodegradation of toluene

The doping of Co introduces a new energy level, generates more electron capture centers, and separates more electron-hole pairs. Figure 7 shows the photocatalytic degradation mechanism of toluene using Co-TiO_2/RGO. After being supported on graphene, the larger specific surface area further improves the photocatalytic activity of the catalyst. Toluene, used as the model pollutant, is firstly absorbed on the surface of Co-TiO_2/RGO. After that, Co-TiO_2/RGO is activated by light and the photogenerated electron-hole pairs are separated, and the photogenerated electrons are quickly transferred to the graphene surface. Then a series of reactions occur with oxygen molecules and water molecules (Eq. 1 - 3). After that, the active ·OH and $\cdot O_2^-$ react with the toluene adsorbed on the graphene aerogel to undergo a photocatalytic oxidation reaction, and finally achieve the effect of degrading pollutants.

$$\text{photocatalyst} + h\nu \rightarrow h^+ + e^- \quad (1)$$

$$h^+ + H_2O \rightarrow H^+ + OH^- \quad (2)$$

$$h^+ + OH^- \rightarrow \cdot OH \quad (3)$$

Figure 7. The photocatalytic degradation mechanism of toluene using Co-TiO_2/RGO.

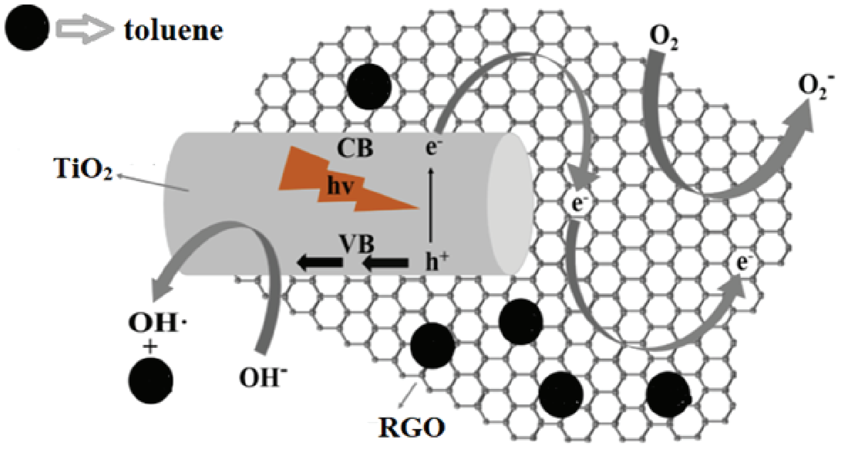

4.Conclusions

The Co-TiO_2/RGO was prepared by electrospinning, heating and freeze-drying. Toluene was used as a model pollutant, and the photocatalytic degradation experiment was carried out to evaluate the performance of the catalyst. Results show that under the conditions of Co doping molar ratio of 1%, calcination temperature of 600℃ for 4 h, gas residence time of 100 min, relative humidity of 100%, and the loading amount of Co/TiO_2 molar ratio of 1%, the degradation percentage of toluene of Co-TiO_2/RGO photocatalyst was the highest, up to 99.1%. This study confirms the possibility of synthesizing Co-TiO_2/RGO for the degradation of pollutants from air.

Funding

This study is financially supported by Science and Technology Commission of Shanghai Municipality (21WZ2501500), and the China Scholarship Council (CSC) scholarship (202106810008).

Conflict of Interests

The author(s)declare(s) that there is no conflict of interest regarding the publication of this paper.

References

[1] McDonald, B. C., Gouw, J. A. d., Gilman, J. B., Jathar, S. H., Akherati, A., Cappa, C. D., ... & Trainer, M. (2018). Volatile chemical products emerging as largest petrochemical source of urban organic emissions. Science, 359(6377), 760-764.

[2] Feng, Q., Liu, B., Ji, J., Li, K., Zhang, B., & Huang, H. J. A. S. S. (2021). Enhanced photo-degradation of gaseous toluene over MnOx/TiO2/activated carbon under a novel microwave discharge electrodeless lamps system. Journal of Hazardous Materials, 547, 148955.

[3] Fujishima, A., & Honda, K. (1972). Electrochemical Photolysis of Water at a Semiconductor Electrode. Nature, 238(5358), 37-38.

[4] Li, P., Wang, M., Huang, S., & Su, Y. (2021). Phosphorus- and fluorine-co-doped carbon nitride: modulated visible light absorption, charge carrier kinetics and boosted photocatalytic hydrogen evolution. Dalton Transactions, 50(40), 14110-14114.

[5] Luo, Z., Ye, X., Zhang, S., Xue, S., Yang, C., Hou, Y., ... & Wang, X. (2022). Unveiling the charge transfer dynamics steered by built-in electric fields in BiOBr photocatalysts. Nature Communications, 13(1), 2230.

[6] Li, Q., & Li, F.-t. (2020). Recent advances in surface and interface design of photocatalysts for the degradation of volatile organic compounds. Advances in Colloid and Interface Science, 284, 102275.

[7] Low, J., Zhang, L., Zhu, B., Liu, Z., & Yu, J. (2018). TiO2 Photonic Crystals with Localized Surface Photothermal Effect and Enhanced Photocatalytic CO2 Reduction Activity. ACS Sustainable Chemistry & Engineering, 6(11), 15653-15661.

[8] Wang, P., Deng, P., & Cao, Y. (2022). Edge-sulfonated graphene-decorated TiO2 photocatalyst with high H2-evolution performance. International Journal of Hydrogen Energy, 47(2), 1006-1015.

[9] Li, T., Abdelhaleem, A., Chu, W., Pu, S., Qi, F., & Zou, J. (2021). S-doped TiO2 photocatalyst for visible LED mediated oxone activation: Kinetics and mechanism study for the photocatalytic degradation of pyrimethanil fungicide. Chemical Engineering Journal, 411, 128450.

[10] Bhattacharyya, K., Mane, G. P., Rane, V., Tripathi, A. K., & Tyagi, A. K. (2021). Selective CO2 Photoreduction with Cu-Doped TiO2 Photocatalyst: Delineating the Crucial Role of Cu-Oxidation State and Oxygen Vacancies. The Journal of Physical Chemistry C, 125(3), 1793-1810.

[11] Kamble, R. J., Gaikwad, P. V., Garadkar, K. M., Sabale, S. R., Puri, V. R., & Mahajan, S. S. (2022). Photocatalytic degradation of malachite green using hydrothermally synthesized cobalt-doped TiO2 nanoparticles. Journal of the Iranian Chemical Society, 19(1), 303-312.

[12] Karafas, E. S., Romanias, M. N., Stefanopoulos, V., Binas, V., Zachopoulos, A., Kiriakidis, G., & Papagiannakopoulos, P. (2019). Effect of metal doped and co-doped TiO2 photocatalysts oriented to degrade indoor/outdoor pollutants for air

quality improvement. A kinetic and product study using acetaldehyde as probe molecule. Journal of Photochemistry and Photobiology A: Chemistry, 371, 255-263.

[13] Yang, J., Shi, C., Dong, Y., Su, H., Sun, H., Guo, Y., & Yin, S. (2022). Efficient hydrogen generation of vector Z-scheme CaTiO3/Cu/TiO2 photocatalyst assisted by cocatalyst Cu nanoparticles. Journal of Colloid and Interface Science, 605, 373-384.

[14] Low, J., Dai, B., Tong, T., Jiang, C., & Yu, J. (2019). In Situ Irradiated X-Ray Photoelectron Spectroscopy Investigation on a Direct Z-Scheme TiO2/CdS Composite Film Photocatalyst. Advanced Materials, 31(5), 1807920.

[15] Li, X., Yu, J., Li, G., Liu, H., Wang, A., Yang, L., ... & Liu, S. (2018). TiO2 nanodots anchored on nitrogen-doped carbon nanotubes encapsulated cobalt nanoparticles as photocatalysts with photo-enhanced catalytic activity towards the pollutant removal. Journal of Colloid and Interface Science, 526, 158-166.

[16] Kusiak-Nejman, E., Wanag, A., Kapica- Kozar, J., Kowalczyk, Ł., Zgrzebnicki, M., Tryba, B., Przepiórski, J., Morawski, A. W. (2020). Methylene blue decomposition on TiO2/reduced graphene oxide hybrid photocatalysts obtained by a two-step hydrothermal and calcination synthesis. Catalysis Today, 357, 630-637.

[17] Padmanabhan, N. T., Thomas, N., Louis, J., Mathew, D. T., Ganguly, P., John, H., & Pillai, S. C. (2021). Graphene coupled TiO2 photocatalysts for environmental applications: A review. Chemosphere, 271, 129506.

[18] Padmanabhan, N. T., Jayaraj, M. K., & John, H. (2020). Graphene hybridized high energy faceted titanium dioxide for transparent self-cleaning coatings. Catalysis Today, 348, 63-71.

[19] Song, Y., Ling, L., Westerhoff, P., & Shang, C. (2021). Evanescent waves modulate energy efficiency of photocatalysis within TiO2 coated optical fibers illuminated using LEDs. Nature Communications, 12(1), 4101.

[20] Xie, J., Xu, M., Wang, R., Ye, S., & Song, X. (2021). Three-dimensional porous spherical TiO2–Bi2WO6 decorated graphene oxide nanosheets photocatalyst with excellent visible light catalytic degradation of ethylene. Ceramics International.

[21] Song, Y., Ling, L., Westerhoff, P., & Shang, C. (2021). Evanescent waves modulate energy efficiency of photocatalysis within TiO2 coated optical fibers illuminated using LEDs. Nature Communications, 12(1), 4101.

[22] Pasini, S. M., Valério, A., Yin, G., Wang, J., de Souza, S. M. A. G. U., Hotza, D., & de Souza, A. A. U. (2021). An overview on nanostructured TiO2–containing fibers for photocatalytic degradation of organic pollutants in wastewater treatment. Journal of Water Process Engineering, 40, 101827.

[23] Zheng, X., Liu, Y., Liu, X., Li, Q., & Zheng, Y. (2021). A novel PVDF-TiO2@g-C3N4 composite electrospun fiber for efficient photocatalytic degradation of tetracycline under visible light irradiation. Ecotoxicology and Environmental Safety, 210, 111866

[24] Chen, H.-J., Yang, Y.-L., Zou, X.-X., Shi, X.-L., & Chen, Z.-G. (2022). Flexible hollow TiO2@CMS/carbon-fiber van der Waals heterostructures for simulated-solar light photocatalysis and photoelectrocatalysis. Journal of Materials Science & Technology, 98, 143-150.

[25] Jiang, M., Zhang, M., Wang, L., Fei, Y., Wang, S., Núñez-Delgado, A., Bokhari, A., Race, M., Khataee, A., Klemeš, J. J., Xing, L., & Han, N. (2022). Photocatalytic degradation of xanthate in flotation plant tailings by TiO2/graphene nanocomposites. Chemical Engineering Journal, 431, 134104.

[26] Purabgola, A., Mayilswamy, N., & Kandasubramanian, B. (2022). Graphene-based TiO2 composites for photocatalysis & environmental remediation: synthesis and progress. Environmental Science and Pollution Research, 29(22), 32305-32325.

[27] Chen, L., Li, N., Zhang, M., Li, P., & Lin, Z. (2017). Effect of preparation methods on dispersion stability and electrochemical performance of graphene sheets. Journal of Solid State Chemistry, 249, 9-14.

[28] Aphairaj, D., Wirunmongkol, T., Pavasupree, S., & Limsuwan, P. (2011). Effect of calcination temperatures on structures of TiO2 powders prepared by hydrothermal method using Thai leucoxene mineral. Energy Procedia, 9, 539-544.

[29] Chi, M., Sun, X., Lozano-Blanco, G., & Tatarchuk, B. J. (2021). XPS and FTIR investigations of the transient photocatalytic decomposition of surface carbon contaminants from anatase TiO2 in UHV starved water/oxygen

environments. Applied Surface Science, 570, 151147.

[30] Li, Y., Wang, C., Song, M., Li, D., Zhang, X., & Liu, Y. (2019). TiO2-x/CoOx photocatalyst sparkles in photothermocatalytic reduction of CO2 with H2O steam. Applied Catalysis B: Environmental, 243, 760-770.

[31] Gong, B., Luo, X., Bao, N., Ding, J., Li, S., & Yi, J. (2014). XPS study of cobalt-doped TiO2 films prepared by pulsed laser deposition. Surface and Coatings Technology, 46(10-11), 1043-1046.

[32] Saravanakumar, K., Fayyaz, A., Park, S., Yoon, Y., Kim, Y. M., & Park, C. M. (2021). Hierarchical CoTiO3 microrods on Ti3C2Tx MXene heterostructure as an efficient sonocatalyst for bisphenol A degradation. Journal of Molecular Liquids, 344, 117740.

[33] Yang, G., Yan, W., Wang, J., & Yang, H. (2014). Fabrication and characterization of CoTiO3 nanofibers by sol–gel assisted electrospinning. Materials Letters, 122, 117-120.

[34] Habibi, M. H., & Shojaee, E. (2020). Synthesis of a heterojunction CoTiO3/Co3O4 nano-composite thin film with superior photocatalytic activity and reusability: Effect of calcination temperature on phase transformation and effect of oxidants on enhanced degradation of Indo Light Blue dye. Spectrochimica Acta Part A: Molecular and Biomolecular Spectroscopy, 229, 117796.

[35] Zou, Z., Ye, J., Sayama, K., & Arakawa, H. (2001). Direct splitting of water under visible light irradiation with an oxide semiconductor photocatalyst. Nature, 414(6864), 625-627.

[36] Tang, J., Zou, Z., & Ye, J. (2003). Photophysical and photocatalytic properties of AgInW2O8. The Journal of Physical Chemistry B, 107(51), 14265-14269.

[37] Umebayashi, T., Yamaki, T., Itoh, H., & Asai, K. (2002). Analysis of electronic structures of 3d transition metal-doped TiO2 based on band calculations. Journal of Physics and Chemistry of Solids, 63(10), 1909-1920.

[38] Wang, D., Zou, Z., & Ye, J. (2003). A new spinel-type photocatalyst BaCr2O4 for H2 evolution under UV and visible light irradiation. Chemical Physics Letters, 373(1), 191-196.

[39] Miyoshi, A., Nishioka, S., & Maeda, K. (2018). Water splitting on rutile TiO2-based photocatalysts. Chemistry – A European Journal, 24(69), 18204-18219.

[40] Lee, G.-J., Anandan, S., Masten, S. J., & Wu, J. J. (2016). Photocatalytic hydrogen evolution from water splitting using Cu-doped ZnS microspheres under visible light irradiation. Renewable Energy, 89, 18-26.

[41] Ohno, T., Sarukawa, K., & Matsumura, M. (2001). Photocatalytic activities of pure rutile particles isolated from TiO2 powder by dissolving the anatase component in HF solution. The Journal of Physical Chemistry B, 105(12), 2417-2420.

Supporting Information

S1. Experimental

S1.1 Chemicals

Analytical grade reagents including HNO_3, tetra-n-butyl titanate, absolute ethanol, ethylenediamine, and cobalt nitrate hexahydrate and sodium tetraborate decahydrate were obtained from Sinopharm Chemical Reagent Co., Ltd. Reduced graphene oxide was obtained from Jiangsu Yueda Group Co., Ltd. Polyvinylpyrrolidone of analytical grade was obtained from Aladdin Biochemical Technology Co., Ltd. All these chemicals were without further purification, and experimental solutions were prepared with deionized water.

S1.2 Synthesis of Co-TiO_2 fiber using electrospinning

Firstly, 5 g of polyvinyl pyrrolidone was added to 20 g of absolute ethanol to obtain precursor A. Secondly, 15 mL of glacial acetic acid and 15 mL of tetrabutyl titanate were added to 15 mL of ethanol to obtain precursor B. Then, PVP/Co-TiO_2 fiber was obtained by electrospinning the mixture of A and B on the negative iron plate. After that, the PVP/Co-TiO_2 fiber was calcined in a muffle furnace for 4 hours, and the temperature was set at 500°C, 600°C, 700°C, and 800°C, respectively. After the calcination, it was cooled to room temperature, and Co-TiO_2 fiber was obtained after grinding.

S1.3 Synthesis of Co-TiO_2/RGO

60 mL of graphene oxide dispersion was mixed with 0.36 mL of ethylenediamine and 0.003 g of sodium borate. The mixture was sonicated for 10 minutes and then reacted in a vacuum oven. After that, the mixture was soaked in an ethanol aqueous solution for 3 hours to obtain a clean graphene hydrogel. According to a mass ratio of Co-TiO_2 fiber and graphene of 5:100, the Co-TiO_2 fiber and graphene gel were mixed uniformly, and then placed in a vacuum freeze dryer for 35 h to obtain Co -TiO_2/RGO.

S1.4 Material characterization

Morphology of the samples was characterized by a Hitachi S-4800 scanning electron microscope (SEM). Elemental composition of materials was analyzed using an EDAX TEAM Apollo Energy Dispersive Spectroscopy (EDS). Crystal structure of the samples was determined by a Bruker D8 Advanced X-ray diffractometer (XRD). Ultraviolet-visible (UV-vis) absorption spectra of the samples were obtained from a Shimadzu UV-2550 spectrophotometer. The Brunauer-Emmett-Teller (BET) surface area of samples were measured by a TriStar II analyzer. The photoluminescence (PL) spectrums of materials were tested with a Hitachi F7000 Fluorescence Spectrophotometer.

S1.5 Photocatalytic degradation experiments

The processes and devices for photocatalytic degradation of toluene is shown in Figure S1, which mainly includes the gas distribution part, gas flow control part, photocatalytic degradation part, gas sampling and detection part, and an exhaust gas treatment part.

Figure S1. The process of photocatalytic degradation of toluene.

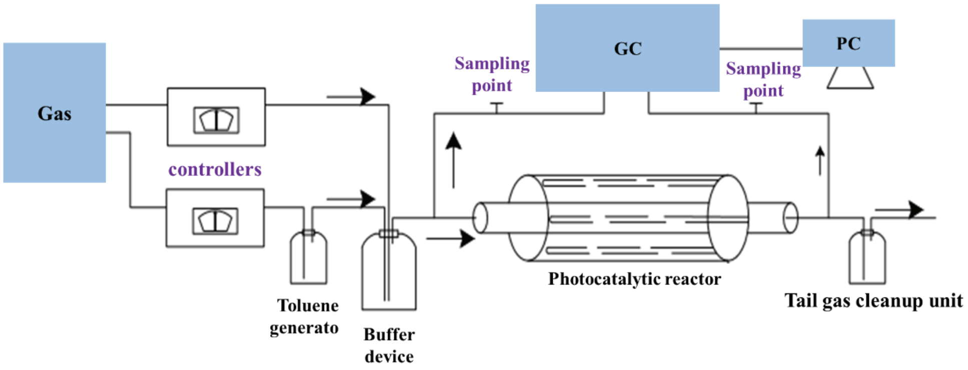

Toluene standard gas (300 ppm) was used as the model pollution gas. The simulated exhaust gas distribution is divided into 2 routes, which are controlled by the flow controllers in the gas-phase photocatalytic system. Samples were taken from the inlet and outlet and the gas samples were detected by a Shimadzu GC9800 gas chromatograph (GC). The calculation formula for the removal percentage of toluene is as follows:

$$\eta(\%) = \frac{C_{in} - C_{out}}{C_{in}} \times 100\% \qquad (1)$$

in which C_{in} and C_{out} are the concentrations of toluene at the gas inlet and the outlet, η is the removal percentage. All the experiments are conducted for 3 times, and the mean value is used for further analysis.

Figure S2. The XPS figure of Co element.

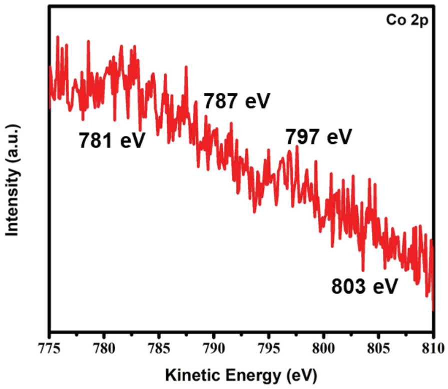

Table S1. Specific surface area, pore size and pore volume of three photocatalysts.

Photocatalysts	**Specific surface area (m^2/g)**	**Pore size (nm)**	**Pore volume (cm3/g)**
TiO_2	142.37	33.10	0.311
Co-TiO_2	131.56	37.91	0.387
Co-TiO_2/RGO	168.86	21.66	0.401

Table S2. Toluene removal by different catalyst.

Catalyst	**Degradation percentage (%)**	**Condition**	**Reference**
TiO_2–Cu_2O	78.3%	171.6 mg/m^3, 30 mg catalyst, xenon lamp of 180 W, 3h	[1]
TiO_2 (Evonik P25, Cristal PC105, Kronos 1077, and Cristal AT-1); Support: flat glass disk	52% for P25; 50% for PC105; 46% for Kronos1077; and 46% for Cristal AT-1	400 ppm, 50 mg catalyst, 40% relative humidity, iron halogenide lamp of 500 W, 6 h	[2]
TiO_2/SiO_2	65%	700 ppm, 0.68 g catalyst, 50% relative humidity, UV Lamp of 3 W, 3 h	[3]
Activated carbon fiber coated TiO_2	86%	500 ppb, 40% relative humidity, mercury lamp of 15 W, 3 h	[4]
Co-TiO_2/RGO	99.1%	1% Co, 1g catalyst, 100% relative humidity, 100min	This study

References

[1] Cheng, Y., Gao, X., Zhang, X., Su, J., Wang, G., & Wang, L. (2018). New Journal of Chemistry, 42(1), 9252-9259.

[2] Bianchi, C. L., Gatto, S., Pirola, C., Naldoni, A., Di Michele, A., Cerrato, G., Crocellà, V., & Capucci, V. (2014). Applied Catalysis B: Environmental, 146, 123-130.

[3] Paušová, Š., Pacileo, L., Baudys, M., Hrubantová, A., Neumann-Spallart, M., Dvoranová, D., Brezová, V., & Krýsa, J. (2020). Catalysis Today.

[4] Guo, T., Bai, Z., Wu, C., & Zhu, T. (2008). Frontiers of Environmental Science & Engineering in China, 2(1), 224-229.